Research Article Vol. 3, No. 9 / 15 September 2020 / OSA Continuum 2407

# In-line evanescent-field-coupled THz bandpass mux/demux fabricated by additive layer manufacturing technology

A. I. Hernandez-Serrano,[1] Simon J. Leigh,[2] and Emma Pickwell-MacPherson[1,*]

[1]Department of Physics, University of Warwick, Gibbet Hill Road, Coventry, CV47AL, UK
[2]School of Engineering, University of Warwick, Gibbet Hill Road, Coventry, CV47AL, UK
[*]e.macpherson@warwick.ac.uk

**Abstract:** In this research, we present the design, fabrication, and experimental validation of 3D printed bandpass filters and mux/demux elements for terahertz frequencies. The filters consist of a set of in-line polystyrene (PS) rectangular waveguides, separated by 100 µm, 200 µm, and 400 µm air gaps. The principle of operation for the proposed filters resides in coupled-mode theory. Q-factors of up to 3.4 are observed, and additionally, the experimental evidence demonstrates that the Q-factor of the filters can be improved by adding fiber elements to the design. Finally, using two independent THz broadband channels, we demonstrate the first mux/demux device based on 3D printed in-line filters for the THz range. This approach represents a fast, robust, and low-cost solution for the next generation of THz devices for communications.



## 1. Introduction

Additive manufacturing technology, also known as 3D printing, is a valuable technique for the fabrication of complex optical components for the terahertz (THz) range of frequencies [1,2]. The impact of such devices has spread across a wide range of areas, including skin characterisation [3], microscopy [4], polarization control [5], photonic crystals [6,7], beam formation [8,9], and THz fibers [10,11], just to name few. The success of rapid prototyping in the THz area is due to the ability to create complex structures within a few minutes, giving researchers the freedom to explore exotic geometries [12]. Due to the increasing interest in applications of THz light, devices able to manipulate this radiation are becoming in higher demand, and fortunately, 3D printing offers a solution. Bandpass filters are some of the key components needed for the manipulation of THz light. Designs to produce them hitherto incorporate fundamental principles from guided-mode resonances [13], Bragg resonators [11,14], and two-dimensional periodic structures [6] among others [1,2,15]. Coupled mode waveguides have proved useful in the microwave regime [16–18], and recently this technology has been demonstrated at THz frequencies [19,20]. For the microwave region, micro-strip technologies are used; however, this method is not suitable for the THz range. In this paper, coupled in-line 3D printed filters are presented as a solution for manipulating THz light. These filters give a Q-factor enhancement depending on the number of fibers concatenated in the design. Finally, we use two filters to give the first demonstration of THz multiplexing/demultiplexing using 3D printed co-directional dielectric waveguides, proving that this approach can be used not only to filter THz radiation but also to combine/separate the frequency components of two independent broadband input channels. This method, therefore, represents a valuable approach for the next generation of passive photonic devices for the THz band, making it highly attractive for research in the field of communications.

#399389 https://doi.org/10.1364/OSAC.399389
Journal © 2020 Received 3 Jun 2020; revised 8 Jul 2020; accepted 8 Jul 2020; published 25 Aug 2020

OSA CONTINUUM

## 2. Design and fabrication

The devices were made out of fused polystyrene filaments ($n_{PS}$=1.56 at 0.12 THz [19,21]) with a cross-section of 1.2 mm by 1.2 mm and were fabricated using the Ultimaker3 3D printer with a vertical resolution of 0.1 mm and a nozzle hole of 0.4 mm. The filter consists of two to five rectangular waveguides (cross-section 1.2 mm by 1.2 mm) separated laterally by 100 µm, 200 µm and 400 µm air gaps ($a$ indicated in Fig. 1) and shifted longitudinally by 25 mm (overlapping length). A schematic diagram of the printed filter is shown in Fig. 1 along with a photograph of the printed filters and a single fiber element. The principle of operation of the dielectric filters relies on the coupling mode theory [22,23].

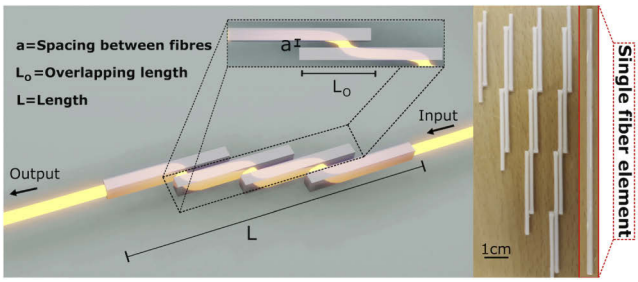


**Fig. 1.** Schematic diagram of the 3D printed in line bandpass filter. Photo (right) of four filters with different numbers of fibers for a 400 µm spacing. A single fiber element is also shown.

When two dielectric waveguides are placed in close proximity, the light propagating originally in one waveguide can leak completely to the other via mode coupling between the lowest odd and even modes [22,23]. The transcendental equations for the propagation of the even and odd modes in the $(K_1 d, \gamma d)$ space are given by:

$$-\frac{\gamma}{n_{air}^2} tanh\ tanh\ (0.5\gamma a)\ + \frac{K_1}{n_{PS}^2} tan\ tan\ (K_1 d)\ - \frac{\gamma}{n_{air}^2}\left[1 + \frac{\gamma}{K_1}\left(\frac{n_{PS}}{n_{air}}\right)^2 tanh\ tanh\ (\gamma a)\ tan\ tan\ (\gamma d)\right] = 0 \quad (1)$$

and

$$1 - \frac{K_1}{\gamma}\left(\frac{n_{air}}{n_{PS}}\right) tanh\ tanh\ (0.5\gamma a)\ tan\ tan\ (K_1 d) + \frac{\gamma}{K_1}\left(\frac{n_{PS}}{n_{air}}\right) tan\ tan\ (K_1 d) + \left(\frac{n_{PS}}{n_{air}}\right)^2 tanh\ tanh\ (0.5\gamma a)\ = 0, \quad (2)$$

where $d$=1.2 mm is the waveguide cross-section, $K_1$ and $\gamma$ are the propagation constant and the extinction coefficient, respectively [22,23]. We solve Eq. (1) and Eq. (2) to find the solutions for the propagation of the even and odd modes respectively in the $(K_1 d, \gamma d)$ space. In our design, the propagation constant for the even/odd modes $\beta_{even/odd}$ can be found using $\beta_{odd/even}^2 = K_1^2 - (n_{PS}k)^2$, where $k$ is the propagation constant in vacuum [22,23]. Then, the coupling length is defined as the distance in which the phase difference between the lowest even and odd is exactly $\pi$ [22,23], i.e.

$$L_c = \frac{\pi}{\beta_{even} - \beta_{odd}}. \quad (3)$$

From Eqs. (1) and (2) it is clear that $\beta_{even/odd}$ as well as $L_c$ depend on the separation between fibers ($a$) for a given frequency. In our design shown in Fig. 1, we define the overlapping length ($L_o$) as the longitudinal distance in which the light inside one fiber can interact with the neighbour fiber. This distance has been kept fixed to 25 mm. Only the light with a frequency that meets the condition $L_c(a, f) = L_o$, for a given spacing ($a$) and frequency ($f$), will be propagated efficiently from the input port to the output port. This phenomenon is used for band-pass filtering. In Fig. 2(a) the coupling length for frequencies between 110 GHz to 200 GHz and separation

OSA CONTINUUM

between fibers of 0.1 mm to 0.4 mm is plotted as a surface, along with the plane at $L_o$ =25 mm (horizontal yellow plane). The intersection between the surface and the plane (white curve) gives $L_c(a,f) = L_o$, indicating the frequencies able to propagate inside the in-line structure at different spacings. Figure 2(b) is a top view of (a) with the intersection line. This highlights that the filters have a centre frequency of operation close to 120 GHz, 160 GHz and 180 GHz for the 400 µm, 200 µm and 100 µm gaps respectively. These values were also confirmed by numerical simulations.

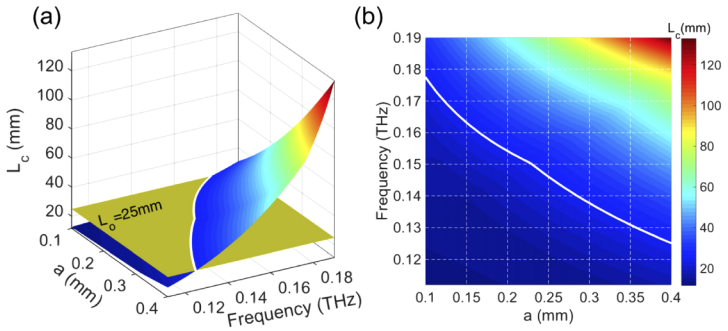


**Fig. 2.** (a) Coupling length surface as function of frequency and spacing between fibers. The horizontal plane represents the 25 mm overlapping distance ($L_o$). (b) Top view of (a) without the horizontal plane.

In Fig. 3, numerical simulations for the electric field intensity are shown for the 200 µm spacing filter. The numerical results were carried out using COMSOL Multiphysics and the Electromagnetic Waves, Frequency Domain (EWFD) module. The discretization of the mesh was λ/10 in order to ensure accuracy and scattering boundary conditions were employed. The array in this simulation consists of four fibers. From the numerical results, the performance of the filter is explained as follows: only the frequency of 160 GHz fulfils the condition $L_c(200\ \mu m) = L_o$, then, the light can be coupled within every adjacent fiber and guided to the exit of the filter as shown in Fig. 3(b). However, when the coupling length of the incident beam does not match the condition, a significant fraction of the light is leaked out at the end of every fiber. From these results, it is clear that a considerable amount of energy is lost at the end of the first fiber, while the rest of the energy is lost at every subsequent fiber. Additionally, in light of these results, it is intuitive to notice that adding more fiber steps in the design will help to remove the non-resonant frequencies

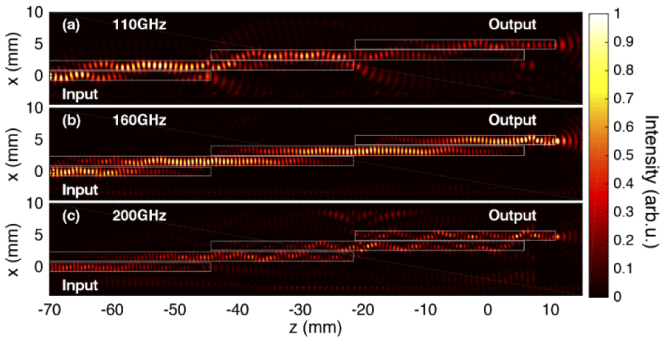


**Fig. 3.** Electric field intensity simulations for the 200 µm spaced filter and four dielectric fibers at (a) 110 GHz, (b) 160 GHz and (c) 200 GHz. The E-field travels from left to the right of the simulation window.

OSA CONTINUUM

more efficiently. This process increases the Q-factor of the resultant filter. To demonstrate experimental evidence of this process, the following variables are investigated: three different spacings (100 µm, 200 µm and 400 µm) and four different numbers of fibers (two, three, four and five). A total of twelve filters were studied, and the transmitted spectra are analysed. Each of the twelve fibers was printed with the same length and same cross-section and was measured individually to meaningfully compare the transmitted light through a single fiber and the filters (array of fibers).

## 3. Experimental results

For the experimental procedure, the fiber-coupled TeraSmart THz spectrometer from Menlo systems was used. The system emits short THz pulses with a temporal duration of approximately 1 ps exhibiting a frequency content up to 5 THz with a dynamic range of 90 dB. The schematic of the experimental setup is presented in Fig. 4. The THz radiation was coupled into the filters using two pairs of TPX lenses with a 1.5-inch diameter and 50 mm focal length. Additionally, two metallic apertures were used in order to hold the filter in focus and to prevent direct transmission from the transmitter to the receiver.

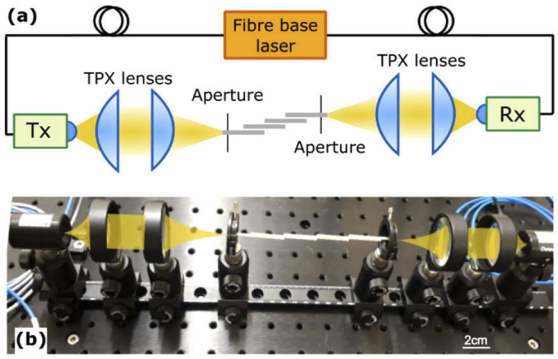


**Fig. 4.** (a) Schematic diagram of the experimental setup. The THz probes were arranged in a transmission configuration. THz light is guided using four TPX lenses (1.5-inch diameter) with 50 mm focal length. Metallic apertures were used to hold the filter in position and to prevent direct transmission of THz radiation from the emitter (Tx) to the receiver (Rx). (b) Photograph of the experimental apparatus.

Each filter tip was placed at the focal position of the second and third lenses (from left to right). Transmission spectra of the five fiber filters with different spacings, as well as that of 200 µm spacing filters with different numbers of fibers, are plotted in Figs. 5(a) and 5(b), respectively. Transmission spectra of the five fiber filters with different spacings, as well as that of 200 µm spacing filters with different numbers of fiber, are plotted in Figs. 5(a) and 5(b), respectively.

The spectra were calculated by taking the absolute ratio of the spectra transmitted through the twelve filters $FFT(E_{samp}(t))$ and the spectra transmitted through the twelve single rectangular fiber elements with the same filter length, labelled L in Fig. 1 $FFT(E_{ref}(t))$ according with the equation, $|Transmission(\omega)| = \left|\frac{FFT(E_{samp}(t))}{FFT(E_{ref}(t))}\right|$. This equation highlights the propagation losses the multi-fibers filter may have relative to the single fiber case. From Fig. 5(b), it is clear that the bandpass region becomes narrower and has a higher Q-factor as the number of fibers in the filter increases. To completely eliminate frequencies with small coupling efficiency, the addition of more fibers is necessary as the losses will be multiplied in every coupling such that the signals will become negligible at the output channel. Therefore, the higher the number of fibers, the lower the transmission of low efficiency frequencies. When five fibers are used, the transmission spectra

OSA CONTINUUM

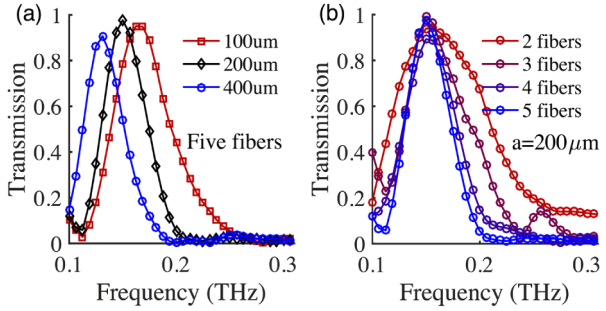


**Fig. 5.** Transmission spectra of filters with (a) five fibers, (b) transmission spectra of the filters with two, three, four and five fibers keeping the spacing between fibers constant (a=200$\mu m$). The transmission was calculated by taking the ratio between the transmitted light through every individual filter and the transmitted radiation through a single rectangular fiber element with the same length of the filter.

for three different spacings (100 µm, 200 µm and 400 µm) are all higher than 90%, relative to the single fiber transmission case, as shown in Fig. 5(a). In order to quantify the improvement of the Q-factor as a function of the number of fibers, a Gaussian curve was fitted to the transmission spectrum of every filter. The Q-factor has been calculated using the formula, $Q = \frac{f_c}{\Delta f}$, where $f_c$ is the central frequency (resonance frequency) and $\Delta f$ is the full-width-half-maximum of the bandpass region (bandwidth) of the fitted Gaussian curves. These results are shown in Fig. 6(b).

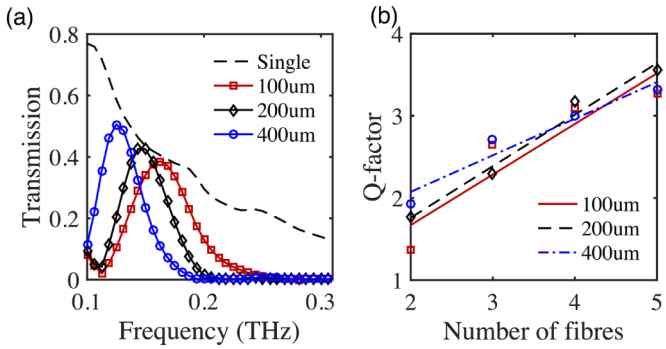


**Fig. 6.** (a) Transmitted THz light relative to the free-space transmission for the 100 µm, 200 µm, 400 µm spaced five fibers filter and single fiber case. (b) Experimental Q-factor as a function of the number of fibers. The straight lines in (a) are linear fits to the experimental Q-factor.

The linear fits to the Q-factor as a function of the number of fibers show that for the 100 µm, 200 µm, 400 µm the increases in the Q-factor per number of fibers are 0.61, 0.62 and 0.44, respectively. In order to fabricate a bandpass filter with a narrower bandwidth region, additional fibers have to be incorporated in the design (more than five in this case). However, for this study, we were limited to a maximum of five fibers as adding more fibers would delay the THz radiation for more than 850 ps, which is the temporal limit of detection of the TeraSmart THz system. To complement this study, an additional measurement was taken for the transmitted THz light through free space, i.e. the filter shown in Fig. 4 was removed, the two TPX lenses were arranged in a confocal geometry and then the THz radiation was recorded. The ratio of the transmitted THz light for the five-fiber filters and single fiber relative to the free space transmission is shown in Fig. 6(b). This plot indicates that transmission efficiencies up to 50% are achieved for these

OSA CONTINUUM

devices relative to free space. The results also show all the losses in the device. These losses are caused by impedance mismatches, scattering, material absorption and coupling efficiencies which represent 50% of the incident E-field. Finally, in Fig. 7, experimental validation of a proposed mux/demux device is presented. The proposed mux/demux consists of two in-line bandpass filters with different spacings (100 µm and 400 µm), separated by a unique fiber used to couple in or out the THz light. A schematic diagram is shown in the insets of Fig. 7.

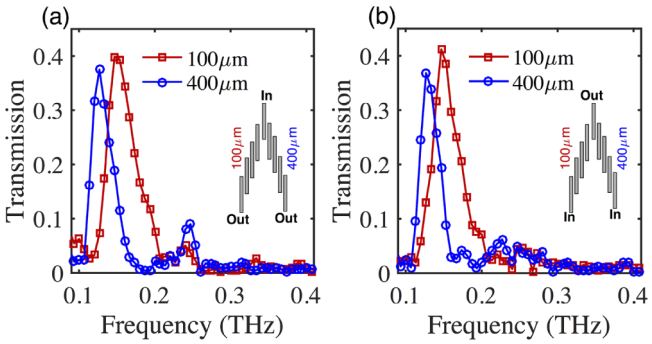


**Fig. 7.** Experimental transmission spectra, compared to the air-reference, for the two filter devices acting as a: (a) demultiplexer and (b) multiplexer. The inset represents the schematic diagram of the mux/demux device as well as the experimental configuration. The spacing between fibers was 100 µm and 400 µm.

A broadband THz light beam was inputted through the single fiber, as shown in the inset Fig. 7(a). Afterwards, placing the receiver at the end of one of the two out ports, two different band regions were recorded. These bands are shown in Fig. 7(a) after passing through the 100 µm arm (red) and the 400 µm arm (blue). Conversely, moving the receiver to the single output, as shown in the inset of Fig. 7(b), while the emitter is aligned in every one of the two input ports, the two spectral regions presented in Fig. 7(b) were recorded. For the first case [Fig. 7(a)] this new geometry performs the function of a demultiplexer (separation of frequencies), meanwhile, for the second case [Fig. 7(b)], the device acts as a multiplexer (different frequencies combined in a single output line). Close to fifty-fifty splitting is obtained with this configuration, similar to other mux/demux approaches [20,24–27]. Additionally, with this approach, the frequency splitting does not require movable parts [25]. Finally, in order to show insight into a practical application of the proposed printed mux/demux, two independent THz broadband input channels are aligned with the input tips of the fibers, as shown in Fig. 8(b). To the best of our knowledge, this is the first study using two independent THz broadband channels for the analysis of a 3D printed mux/demux element using in–line geometry. For this experiment, a minor modification was made to our original design of the mux/demux. This time, one of the input fibers was printed with a curved end to couple the second emitter avoiding cross-talking. It is important to highlight that curve geometry may incur in additional propagation losses. The radius of curvature used here is 17.5 mm, representing additional transmission losses around 1% [19]. A picture of the new design is shown in Fig. 8. Three measurements were taken; first blocking input A while input B is open, then opening input A and keeping input B blocked and finally, both inputs unblocked.

From the transmitted spectra, two spectral regions are evident for the (A=1, B=0) (open diamonds) and (A=0, B=1) (open squares) cases, proving efficient separation of the broadband input spectra. Furthermore, for the two inputs open case (A=1, B=1), the transmitted spectral region now covers a wider region enclosing the two previous spectral bands (dashed black line). Finally, the (A=0, B=1) and (A=1, B=0) curves were numerically added, and the result is represented by the open circles curve. The resulting curve is seen to be in good agreement with the previous result for the (A=1, B=1) case. The experimental evidence demonstrates that the

OSA CONTINUUM

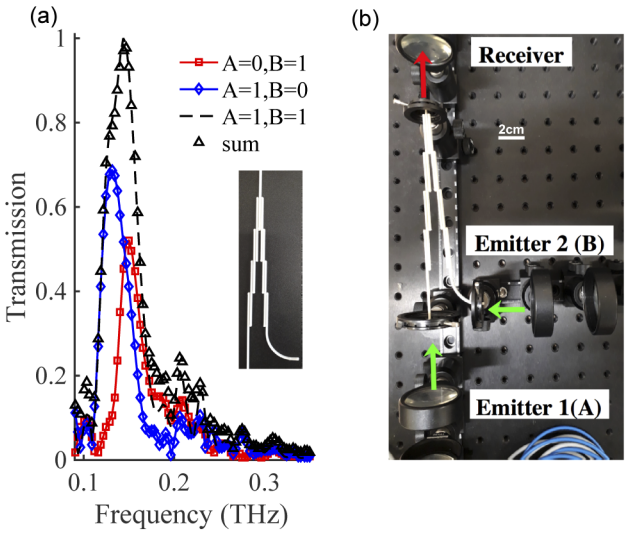


**Fig. 8.** (a) Normalized transmission spectra for the two independent broadband THz input channels experiment. Inset shows a photograph of the finished device. (b) Photograph of the experimental configuration.

proposed printed geometry effectively acts as a multiplexer of two independent input channels, and has valuable characteristics for the fabrication of the next generation of devices for THz communications.

## 4. Conclusions

The performance of a bandpass filter fabricated by 3D printing for the THz range of frequencies is presented here. The principle of operation of the filter is based on coupled-mode theory and the operation frequency of the proposed filter is highly dependent on the spacing between fibers. The experimental results indicate that the Q-factor of the filter can be improved by adding more fiber stages into the design. This is also supported by numerical calculations. Incremental improvement in the Q-factor as a function of the number of fibers was found to be 0.62 units per fiber for the 200 μm spaced filter. Furthermore, connecting two filters by a single fiber, was demonstrated to be a powerful method to multiplex and demultiplex broadband input channels. We envisage that tunable 3D printed mux/demux devices will be able to dynamically change the spacing between fibers making it possible to tune the frequency band of operation. Due to the high flexibility, robustness and low cost given by additive layer manufacturing techniques, we anticipate that this device will be highly valuable for the next generation of THz communication systems.

## Funding

Royal Society Wolfson Merit Award; Engineering and Physical Sciences Research Council (EP/S021442/1).

## Disclosures

The authors declare no conflicts of interest.

OSA CONTINUUM

## Data Availability

The data presented in this paper are available at http://figshare.com/articles/data_dielectric_mux_zip/12115308.

## References


1. J. Sun and F. Hu, "Three-dimensional printing technologies for terahertz applications: A review," Int. J. RF Microw. Comput. Eng. **30**, e21983 (2020).
2. H. Y. Jeong, E. Lee, S.-C. An, Y. Lim, and Y. C. Jun, "3D and 4D printing for optics and metaphotonics," Nanophotonics **9**(5), 1139–1160 (2020).
3. Y. Wang, F. Qi, Z. Liu, P. Liu, W. Li, H. Wu, and W. Ning, "Wideband method to enhance the terahertz penetration in human skin based on a3-D printed dielectric rod waveguide," IEEE Trans. THz Sci. Technol. **9**(2), 155–164 (2019).
4. B. Zhu, S. Vanloocke, J. Stiens, D. De Zutter, A. Elhawil, C. De Tandt, and R. Vounckx, "A novel 3D printed focusing probe in scattering-type scanning near-field millimetre & terahertz wave microscope," in *Proceedings of the 5th European Conference on Antennas and Propagation (EUCAP)*, (IEEE, 2011), pp. 745–748.
5. A. I. Hernandez-Serrano, Q. Sun, E. G. Bishop, E. R. Griffiths, C. P. Purssell, S. J. Leigh, J. Lloyd-Hughes, and E. Pickwell-MacPherson, "Design and fabrication of 3-D printed conductive polymer structures for THz polarization control," Opt. Express **27**(8), 11635–11641 (2019).
6. C. R. Tubío, J. A. Nóvoa, J. Martín, F. Guitián, J. R. Salgueiro, and A. Gil, "Broadband terahertz ZnO photonic crystals fabricated by 3D printing," Ceram. Int. **45**(5), 6223–6227 (2019).
7. X. Zeng, R. Wang, X. Xi, B. Li, and J. Zhou, "3D direct writing of terahertz metamaterials based on TbFeO3 dielectric ceramics," Appl. Phys. Lett. **113**(8), 081901 (2018).
8. C. Liu, J. Liu, L. Niu, X. Wei, K. Wang, and Z. Yang, "Terahertz circular airy vortex beams," Sci. Rep. **7**(1), 3891 (2017).
9. C. Liu, X. Wei, L. Niu, K. Wang, Z. Yang, and J. Liu, "Discrimination of orbital angular momentum modes of the terahertz vortex beam using a diffractive mode transformer," Opt. Express **24**(12), 12534–12541 (2016).
10. K. Nielsen, H. K. Rasmussen, A. J. Adam, P. C. Planken, O. Bang, and P. U. Jepsen, "Bendable, low-loss topas fibers for the terahertz frequency range," Opt. Express **17**(10), 8592–8601 (2009).
11. J. Li, K. Nallappan, H. Guerboukha, and M. Skorobogatiy, "3D printed hollow core terahertz bragg waveguides with defect layers for surface sensing applications," Opt. Express **25**(4), 4126–4144 (2017).
12. S. F. Busch, J. C. Balzer, G. Bastian, G. E. Town, and M. Koch, "Extending the Alvarez-lens concept to arbitrary optical devices: tunable gratings, lenses, and spiral phase plates," IEEE Trans. THz Sci. Technol. **7**(3), 320–325 (2017).
13. M. Ortiz-Martinez, E. Castro-Camus, and A. I. Hernandez-Serrano, "Guided-mode filters for terahertz frequencies fabricated by 3D printing," J. Infrared, Millimeter, Terahertz Waves **40**(7), 731–737 (2019).
14. J. Yuan, T. Ning, H. Li, L. Pei, J. Li, J. Zheng, and L. Wan, "Terahertz filters based on subwavelength polymer waveguide," Results Phys. **13**, 102198 (2019).
15. J. Bomba, J. Suszek, M. Makowski, A. Sobczyk, and M. Sypek, "3-D printed anti-reflection structures for the terahertz region," J. Infrared, Millimeter, Terahertz Waves **39**(1), 24–35 (2018).
16. P. Cheong, S.-W. Fok, and K.-W. Tam, "Miniaturized parallel coupled-line bandpass filter with spurious-response suppression," IEEE Trans. Microwave Theory Techn. **53**(5), 1810–1816 (2005).
17. T. Lopetegi, M. A. Laso, F. Falcone, F. Martin, J. Bonache, J. Garcia, L. Perez-Cuevas, M. Sorolla, and M. Guglielmi, "Microstrip "wiggly-line" bandpass filters with multispurious rejection," IEEE Microw. Wirel. Components Lett. **14**(11), 531–533 (2004).
18. A. Garg, B. Pratap, and D. Gupta, "Design of parallel coupled line bandpass filter," in *2016 Second International Conference on Computational Intelligence & Communication Technology (CICT)*, (IEEE, 2016), pp. 452–454.
19. M. Weidenbach, D. Jahn, A. Rehn, S. Busch, F. Beltrán-Mejía, J. Balzer, and M. Koch, "3D printed dielectric rectangular waveguides, splitters and couplers for 120 GHz," Opt. Express **24**(25), 28968–28976 (2016).
20. Y. Zhang, Y. Xu, C. Tian, Q. Xu, X. Zhang, Y. Li, X. Zhang, J. Han, and W. Zhang, "Terahertz spoof surface-plasmon-polariton subwavelength waveguide," Photonics Res. **6**(1), 18–23 (2018).
21. S. Busch, M. Weidenbach, M. Fey, F. Schäfer, T. Probst, and M. Koch, "Optical properties of 3D printable plastics in the THz regime and their application for 3D printed THz optics," J. Infrared, Millimeter, Terahertz Waves **35**(12), 993–997 (2014).
22. K. Iizuka, "Elements of photonics: Vol.ii: Fiber and integrated optics," (2002).
23. D. M. Pozar, *Microwave Engineering* (John Wiley & Sons, 2009).
24. N. J. Karl, R. W. McKinney, Y. Monnai, R. Mendis, and D. M. Mittleman, "Frequency-division multiplexing in the terahertz range using a leaky-wave antenna," Nat. Photonics **9**(11), 717–720 (2015).
25. K. S. Reichel, R. Mendis, and D. M. Mittleman, "A broadband terahertz waveguide T-junction variable power splitter," Sci. Rep. **6**(1), 28925 (2016).
26. A. Hernandez-Serrano, D. M. Mittleman, and E. Pickwell-MacPherson, "Broadband amplitude, frequency, and polarization splitter for terahertz frequencies using parallel-plate waveguide technology," Opt. Lett. **45**(5), 1208–1211 (2020).
27. L. Jiu-Sheng, L. Han, and Z. Le, "Compact four-channel terahertz demultiplexer based on directional coupling photonic crystal," Opt. Commun. **350**, 248–251 (2015).